

SEHFS: Structural Entropy-Guided High-Order Correlation Learning for Multi-View Multi-Label Feature Selection

Cheng Peng, Yonghao Li*, Wanfu Gao*, *Member, IEEE*, Jie Wen, *Senior Member, IEEE*, and Weiping Ding, *Senior Member, IEEE*

Abstract—In recent years, multi-view multi-label learning (MVML) has attracted extensive attention due to its close alignment to real-world scenarios. Information-theoretic methods have gained prominence for learning nonlinear correlations. However, two key challenges persist: first, features in real-world data commonly exhibit high-order structural correlations, but existing information-theoretic methods struggle to learn such correlations; second, commonly relying on heuristic optimization, information-theoretic methods are prone to converging to local optima. To address these two challenges, we propose a novel method called Structural Entropy Guided High-Order Correlation Learning for Multi-View Multi-Label Feature Selection (SEHFS). The core idea of SEHFS is to convert the feature graph into a structural-entropy-minimizing encoding tree, quantifying the information cost of high-order dependencies and thus learning high-order feature correlations beyond pairwise correlations. Specifically, features exhibiting strong high-order redundancy are grouped into a single cluster within the encoding tree, while inter-cluster feature correlations are minimized, thereby eliminating redundancy both within and across clusters. Furthermore, a new framework based on the fusion of information theory and matrix methods is adopted, which learns a shared semantic matrix and view-specific contribution matrices to reconstruct a global view matrix, thereby enhancing the information-theoretic method and balancing the global and local optimization. The ability of structural entropy to learn high-order correlations is theoretically established, and both experiments on eight datasets from various domains and ablation studies demonstrate that SEHFS achieves superior performance in feature selection.

Index Terms—Multi-view multi-label learning, feature selection, information theory, structural entropy.

I. INTRODUCTION

Multi-label feature selection has been widely applied in image processing, such as medical image recognition [1]

This work was supported in part by the Natural Science Foundation of Sichuan Province under Grant 2025ZNSFSC1497, and in part by the Fundamental Research Funds for the Central Universities under Grants 93K172025K12 and JBK202511004.

Cheng Peng is with the College of Software, Jilin University, Changchun 130012, China; Wanfu Gao is with the College of Computer Science and Technology, Jilin University, Changchun 130012, China. Both authors are also with the Key Laboratory of Symbolic Computation and Knowledge Engineering of the Ministry of Education, Changchun 130012, China (e-mail: pengcheng5523@mails.jlu.edu.cn; gaowf@jlu.edu.cn).

Yonghao Li is with the School of Computing and Artificial Intelligence, Southwestern University of Finance and Economics, Chengdu 611130, China, and also with the Engineering Research Center of Intelligent Finance, Ministry of Education, Chengdu 611130, China (e-mail: liyonghao@swufe.edu.cn).

Jie Wen is the Shenzhen Key Laboratory of Visual Object Detection and Recognition, Harbin Institute of Technology, Shenzhen, Shenzhen 518055, China (email: jiewen_pr@126.com)

Weiping Ding is the School of Artificial Intelligence and Computer Science, Nantong University, Nantong, 226019, China, and also the Faculty of Data Science, City University of Macau, Macau 999078, China. (E-mail: dwp9988@163.com)

Yonghao Li and Wanfu Gao are the corresponding authors.

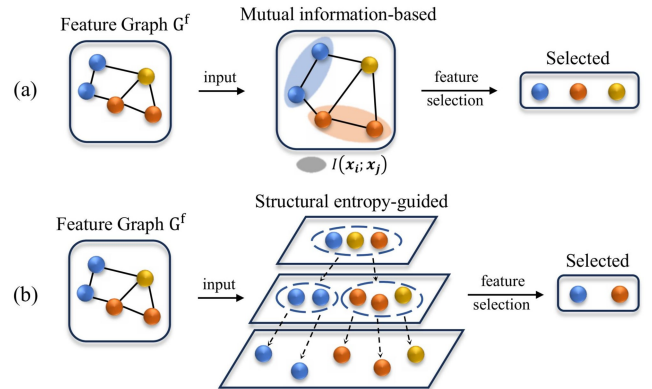


Fig. 1: Concept maps of two type information-theoretic methods. Each ball denotes a feature, and greater color similarity indicates higher correlation. The yellow and red balls show high-order correlation. (a) is existing methods based on mutual information, which are limited to learning low-order correlations; (b) is SEHFS guided by structural entropy, which learns high-order correlations.

and image classification [2]. Recently, with the increasing prevalence of multi-modal data collection, multi-label feature selection is progressively applied in multi-view scenarios [3]. The introduction of multiple views provides more comprehensive and enriched feature semantics, but also introduces additional complexity for feature selection in MVML.

In multi-view scenarios, the core is to explore the relationships among data to balance consistency and complementarity [4]. Data from different views often exhibit shared structure and yield a consensus that captures the most salient information [5]. However, due to inter-view heterogeneity, each view contributes distinctive information, necessitating explicit consideration of complementarity [6].

A major strand of consistency-focused methods aims to identify commonality across views [7], [8]. RRFS [9] measures both inter-view and intra-view information overlap through a view redundancy coefficient, and preserves shared information across views based on information gain. In contrast, researches on complementarity emphasize the differing importance of each view [10], [11]. I^2 VSLC [12] utilizes graph Laplacian to capture the local geometric structure within each view, thereby preserving view-specific characteristics.

However, most existing method adopts linear matrix operations as the final objective function, which makes it difficult for models to capture nonlinear relationships in the space, resulting in weak generalization ability. Moreover, these methods lack effective measures for feature selection [13], [14], making it challenging to directly quantify feature correlations

and redundancy. To address it, some recent methods begin to use information-theoretic methods to select important features.

Most methods utilize mutual information to explore relationships within data and measure nonlinear correlations and redundancy [15], [16], but these methods only capture pairwise and low-order relationships, resulting in limited effectiveness and high computational cost, which are further exacerbated in multi-view scenarios. FLSFE [17] first obtains the overall fuzzy entropy of the label space through label augmentation, and then determines feature importance by evaluating the change in fuzzy entropy before and after adding each feature. However, information-theoretic methods typically rely on heuristic search strategies for feature selection [18], which can easily lead to local optima.

As illustrated in Figure 1, existing information-theoretic methods are predominantly mutual information-based and thus largely restricted to learning low-order feature correlations. Moreover, because they commonly rely on heuristic optimization, they are prone to converging to local optima. To address these two challenges, we propose **Structural Entropy Guided High-Order Correlation Learning for Multi-View Multi-Label Feature Selection (SEHFS)**. The core idea of SEHFS is to convert the feature graph into a structural-entropy-minimizing encoding tree [19], thereby quantifying the information cost of high-order dependencies and enabling the learning of high-order feature correlations beyond pairwise correlations. Concretely, the encoding tree aggregates features characterized by strong high-order redundancy into one cluster and attenuates cross-cluster feature correlations, thus eliminating redundancy inside and between clusters. In addition, we adopt a fusion framework that integrates information theory with matrix methods: a shared semantic matrix and view-specific contribution matrices are learned to reconstruct a global view matrix, which strengthens the information-theoretic modeling and balances global and local optimization. The main contributions of the proposed method are as follows:

- An structural entropy-guided feature selection method based on minimization is proposed, which learns high-order feature correlations and eliminates redundancy, thereby addressing the challenge that existing information-theoretic methods typically learn only low-order correlations and yielding significant achieves superior performance in feature selection.
- An novel information-matrix fusion framework is introduced, which reconstructs a global view matrix to balance multi-view consistency and complementarity, while mitigating the challenge that information-theoretic methods are prone to converging to local optima and balancing the global and local optimization.
- An effective solution to the alternative optimization problem of SEHFS is proposed. Experimental results on eight cross-domain datasets demonstrate that the proposed method outperforms eight state-of-the-art methods.

The structure of this paper is as follows: Section II reviews the related works from previous studies. Section III provides a detailed explanation and optimization strategies of SEHFS. Section IV presents an analysis of the experimental results.

Finally, Section V concludes the paper with a comprehensive summary.

II. RELATED WORK

A. Multi-label Feature Selection

In multi-label scenarios, each sample associates with multiple labels, which makes the label space semantically richer [20]. Research on multi-label feature selection (MLFS) achieves significant progress and mainly follows three directions:

First, some methods are based on manifold learning [21], [22]. They use manifold learning to capture the underlying geometric structures of the feature matrix or label matrix, and perform feature selection via sparse regularization. MIFS [23] decomposes multi-label information into a low-dimensional latent matrix and integrates manifold constraints reflecting local geometry with $\ell_{2,1}$ -norm. MSSL [24] incorporates feature manifold learning via graph regularization and $\ell_{2,1}$ -norm sparsity into a least-squares regression model, obtaining sparse regression coefficients through iterative optimization. SPLDG [25] uses pseudo-label learning to mitigate the incompatibility between true labels and linear mapping, and alternately optimizes feature weights using sparse regularization, dynamic graphs, and manifold learning.

Second, an innovative fusion of sparse norms has been proposed to overcome the limitations of conventional sparse regularization in multi-label settings [26]. SRFS [27] fuses inner product regularization and the $\ell_{2,1}$ -norm to construct a sparse complementary norm, which avoids LASSO's tendency to eliminate useful zero-weight features and reduces feature redundancy caused by the $\ell_{2,1}$ -norm.

Third, some methods utilize information-theoretic methods to evaluate features [28], [29]. SRLG-LMA [30] utilizes fuzzy conditional mutual information to select optimal features based on strong relevant label gain. However, these methods rely on mutual information as the evaluation measure and can only capture pairwise low-order relationships.

There are many similarities between MLFS and multi-view multi-label feature selection (MVMLFS). The primary difference lies in whether multiple views are incorporated. The first two types of MLFS methods can be directly applied to multi-view scenarios by simply merging multiple views into a single view [31], the third type of MLFS methods, due to the high computational cost of mutual information calculations, is difficult to apply to large-scale MVML data [32].

B. Multi-view Multi-label Learning

In multi-view scenarios, data come from different views present diverse semantics, which increases both data diversity and scale [33]. Existing MVML methods strive to balance consistency and complementarity to preserve the comprehensive information. Some methods use reconstruction for view fusion [34], [35]. DHLI [36] focuses on reconstructing the label matrix, decomposing labels into dual-layer hybrid labels, and designing a regularization paradigm incorporating logical operations to establish the mapping between hybrid labels and features. GRAFS [37] focuses on reconstructing

the global view, enhancing the completeness of the global view through anchors and unique contributions, and establishing the mapping from the global view to the label matrix. In addition, embedding techniques are employed to map data into low-dimensional latent matrices, enabling the learning of salient information [38], [39]. MSFS [40] decomposes multi-label information into low-dimensional latent label representations to learn label correlations, constructs local geometric structures within each view to capture intra-view similarity, and applies sparse regularization to achieve mapping.

However, when facing more complex and large-scale data, these methods lack generalization ability in feature selection and struggle to learn high-order feature correlation [41], [42].

III. THE PROPOSED METHOD

Given a multi-view multi-label dataset containing n samples and V views (\mathbf{X}, \mathbf{Y}) , the feature matrix \mathbf{X} consists of $[\mathbf{X}_1; \mathbf{X}_2; \dots; \mathbf{X}_v; \dots; \mathbf{X}_V]$, where v indexes the views ($v \in \{1, \dots, V\}$), $d(v)$ represents the feature dimension of v -th view, and $\mathbf{X}_v \in \mathbb{R}^{n \times d(v)}$ denotes each instance for v -th view. The label matrix $\mathbf{Y} = [y_1, y_2, \dots, y_q] \in \{0, 1\}^{n \times q}$ is denoted for all views, where q is the dimension of label vector. In the label matrix, $\mathbf{Y}_{i,j} = 1$ means that the j -th label is a label of i -th sample. In this section, SEHFS is introduced with its framework shown in Figure 2, which consists of two main components: (1) structural entropy regularization is used to learn high-order feature correlations, aiming to eliminate redundancy and achieve feature selection; (2) a global view matrix is reconstructed through matrix operations, aiming to balance global and local optimization.

A. Structural Entropy guided Feature Selection Regularization

Most existing information-theoretic methods use mutual information to compute correlations either between features or between features and labels. However, mutual information is fundamentally limited to pairwise correlations and only can learn low-order feature correlations. SEHFS utilizes the information-theoretic concept of structural entropy via matrix operations, introducing a structural entropy regularization term which can convert the feature graph into a structural-entropy-minimizing encoding tree and thus learn high-order feature correlations and eliminate redundancy among features.

The definition of encoding tree and structural entropy is presented as follows:

Definition 1 (Encoding Tree): Given a graph $G = (X, A)$, X is the set of input data points, A is the adjacency matrix, denoting the weights of edges. The encoding tree \mathcal{T} for G is a hierarchical partition of X , and satisfies: (1) Each tree node $\alpha \in \mathcal{T}$ corresponds to a subset of data points $T_\alpha \subseteq X$. Especially, for the root node λ of \mathcal{T} , we define the points set associated with as $T_\lambda = X$; For the leaf node γ of \mathcal{T} , T_γ contains only one data points (2) For each non-leaf tree node α in \mathcal{T} , its parent node is denoted as α^- ; (3) For each non-leaf tree node α in \mathcal{T} , the union of the subsets associated with all its child nodes forms a complete partition of T_α . Each tree node describes a partition of the data points X , thereby capturing the connectivity patterns of the graph.

Definition 2 (Structural Entropy): The structural entropy [19] is defined under the graph G and the encoding tree \mathcal{T} as follows:

$$H^{\mathcal{T}}(G) = \sum_{\alpha \in \mathcal{T}, \alpha \neq \lambda} H^{\mathcal{T}}(G, \alpha), \quad (1)$$

$$H^{\mathcal{T}}(G, \alpha) = -\frac{g_\alpha}{\text{vol}(\lambda)} \log_2 \frac{\text{vol}(\alpha)}{\text{vol}(\alpha^-)}, \quad (2)$$

where the cut g_α is the weight sum of edges that connect points inside T_α and points outside, and the volume $\text{vol}(\alpha)$, $\text{vol}(\alpha^-)$, and $\text{vol}(\lambda)$ denote the degrees sum of all data points within T_α , T_{α^-} , and \mathcal{T} .

To generalize structural entropy for feature selection, a feature graph $G^f = (\mathbf{D}, \mathbf{A})$ is constructed, where \mathbf{D} is the nodes set corresponding to all d features, with each feature represented as a node, and \mathbf{A} is the adjacency matrix, where the edge weights reflect the feature correlations. Initially, mutual information between features is calculated and aggregated into a d -dimensional square matrix \mathbf{A} :

$$\mathbf{A}_{i,j} = I(\mathbf{x}_{:,i}; \mathbf{x}_{:,j}). \quad (3)$$

Minimizing structural entropy $H^{\mathcal{T}}(\cdot)$ optimizes the overall topological structure of the feature graph G^f , enabling the learning of high-order feature correlations. By comparing the deviation $\Delta^{\mathcal{T}}$ between structural entropy $H^{\mathcal{T}}(\cdot)$ and ground-truth joint entropy $H^*(\cdot)$, as well as the deviation $\Delta^{(2)}$ between the second-order approximation of ground-truth joint entropy $H^{(2)}(\cdot)$ (which can only learn low-order correlations) and $H^*(\cdot)$, the effectiveness of structural entropy in capturing high-order correlations is demonstrated. The definitions of joint entropy and its second-order approximation are as follows:

$$\begin{aligned} H^*(\cdot) &= \sum_{i=1}^n H(X_i) - \sum_{1 \leq i < j \leq n} I(X_i; X_j) \\ &\quad + \sum_{1 \leq i < j < k \leq n} I(X_i; X_j; X_k) - \dots \\ &\quad + (-1)^{n-1} H(X_1; \dots; X_n), \\ H^{(2)}(\cdot) &= \sum_{i=1}^n H(X_i) - \sum_{1 \leq i < j \leq n} I(X_i; X_j). \end{aligned} \quad (4)$$

To rigorously validate the effectiveness of minimizing structural entropy in capturing high-order feature correlations, we examine two limiting cases that represent the extremes of information dependency. According to information decomposition theory [43], the dependency structure of any complex system can be fundamentally decomposed into a linear combination of synergistic and redundant components. Therefore, a robust method for high-order correlation learning must demonstrate accuracy across the entire spectrum between these two extremes. In this analysis, we define Scenario 1 (S_1) to represent the theoretical limit of maximum synergy, and Scenario 2 (S_2) to represent the limit of maximum redundancy. These scenarios serve as critical benchmarks to establish the theoretical superiority of structural entropy over conventional low-order methods.

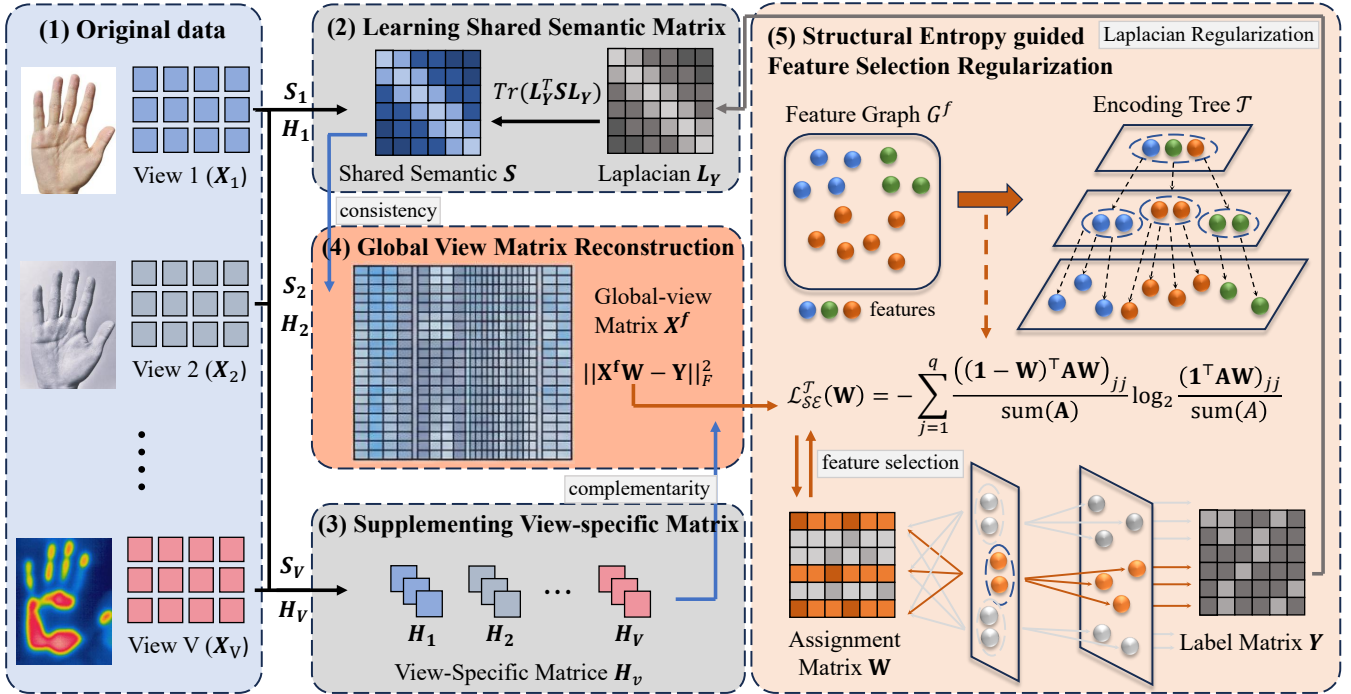


Fig. 2: The framework of SEHFS. Given a multi-view multi-label dataset $[X_1; X_2; \dots; X_V]$, SEHFS first learns the semantic matrix S_v and view-specific matrix H_v from the v -th view X_v . Then, semantic matrices from all views are integrated to form a shared semantic matrix S , whose graph structure is regularized by a graph Laplacian L_Y learned from the label matrix Y . The global view matrix X^f is reconstructed from S and H_v ($v \in \{1; \dots; V\}$), from which a global feature graph G^f is derived. Minimizing the structural entropy of G^f yields an optimal encoding tree \mathcal{T} that learns higher-order correlations and removes redundancy. After mapping Y onto \mathcal{T} produces a more effective, low-redundancy feature selection.

The performance of a method under these extremes is critical: any robust high-order method must maintain accuracy in both regimes. By analyzing these two scenarios, we establish the theoretical superiority of structural entropy over standard low-order approximations.

Scenario 1: Maximum Synergy (The XOR). In this scenario (S_1), we consider a system of three features where X_1 and X_2 are independent uniformly distributed binary variables, and $X_3 = X_1 \oplus X_2$. This configuration represents a state of pure synergy, where information exists solely in the joint distribution of all three variables, with no pairwise correlations.

- *Ground-truth Joint Entropy Analysis:* Since X_1 and X_2 are independent and X_3 is fully determined by them, any pair of variables is sufficient to determine the state of the entire system. Consequently, the true joint entropy is:

$$H^*(S_1) = H(X_1, X_2) = H(X_1) + H(X_2) = 1 + 1 = 2.$$

Despite high-order dependence, the pairwise mutual information vanishes for all pairs: $\forall i \neq j, I(X_i; X_j) = 0$.

- *Second-order Approximation Solution:* Standard low-order methods rely on pairwise statistics. Since all pairwise mutual information terms are zero, the second-order approximation effectively treats the variables as independent:

$$H^{(2)}(S_1) = \sum_i H(X_i) - \sum_{i < j} I(X_i; X_j) = 3 - 0 = 3.$$

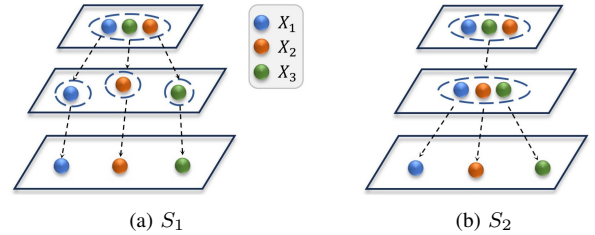


Fig. 3: Structural-entropy-minimizing encoding tree in Scenario 1 and Scenario 2.

This results in a substantial approximation gap of $\Delta^{(2)} = |H^{(2)}(S_1) - H^*(S_1)| = |3 - 2| = 1$, indicating a complete inability to detect the synergistic structure.

- *Structural Entropy Solution:* In the feature graph G^f , the edge weights are determined by mutual information. Since $I(X_i; X_j) = \varepsilon \rightarrow 0$, the optimal encoding tree \mathcal{T} partitions the features into three distinct singleton clusters (as illustrated in Figure 3 (a)). The structural entropy is derived as:

$$H^{\mathcal{T}}(S_1) = 4 \log 3 - 4 \approx 2.338.$$

The resulting metric error is $\Delta^{\mathcal{T}} = |2.338 - 2| \approx 0.338 < 1$. This demonstrates that structural entropy provides a significantly tighter bound than the second-order approximation, even when explicit pairwise signals are absent.

Scenario 2: Maximum Redundancy (The Equality Case).

In this scenario (S_2), we define a system with extreme redundancy involving three identical features: $X_1 = X_2 = X_3$. In this regime, knowledge of any single feature is sufficient to resolve the uncertainty of the entire system.

- *Ground-truth Joint Entropy Analysis:* Since the variables are identical, the joint entropy collapses to the entropy of a single variable. With each feature having unit entropy ($H(X_i) = 1$), the true joint entropy is:

$$H^*(S_2) = H(X_1) = 1.$$

Furthermore, the pairwise mutual information is maximized: $\forall i, j, I(X_i; X_j) = H(X_i) = 1$.

- *Second-order Approximation Solution:* The second-order approximation attempts to correct for independence by subtracting pairwise overlaps. However, in cases of high redundancy, it over-corrects:

$$H^{(2)}(S_2) = \sum_i H(X_i) - \sum_{i < j} I(X_i; X_j) = 3 - 3 = 0.$$

This leads to a physically impossible entropy estimate of zero (implying determinism without observation) and a significant error of $\Delta^{(2)} = |0 - 1| = 1$.

- *Structural Entropy Solution:* Given that all edge weights in G^f equal 1, the strong connectivity drives the optimal encoding tree \mathcal{T} to aggregate all three features into a single cluster (as shown in Figure 3 (b)). The structural entropy is calculated as:

$$H^{\mathcal{T}}(S_2) = 2 \log 3 - 2 \approx 1.169.$$

The corresponding error is $\Delta^{\mathcal{T}} = |1.169 - 1| \approx 0.169 < 1$. This result validates that structural entropy effectively compresses redundant information, maintaining high accuracy where low-order expansions collapse.

Based on the feature graph G^f , a three-layer encoding tree \mathcal{T} is designed to describe correlation patterns among features. The root layer consists of a single root node containing all features; the leaf layer contains d leaf nodes, each representing an individual feature; and the intermediate layer contains q nodes, each corresponding to one of the q clusters in the classification task. An assignment matrix \mathbf{W} is introduced to connect the intermediate layer and the leaf layer, where $\mathbf{W}_{i,j}$ indicates the degree of membership of the i -th feature to the j -th cluster. As the assignment matrix \mathbf{W} is simultaneously learned by a classifier (e.g. $\mathbf{X}\mathbf{W} = \mathbf{Y}$), the q clusters in the intermediate layer can be mapped to the q labels in the label matrix \mathbf{Y} . Thus, the assignment matrix \mathbf{W} serves as a feature selection matrix, where $\mathbf{W}_{i,j}$ represents the degree of membership of the i -th feature to the j -th label. To enhance the representational ability of structural entropy, the row sums of the feature selection matrix \mathbf{W} are constrained to one, thereby ensuring both selection effectiveness and interpretability. The structural entropy of the intermediate layer nodes for the three-tier encoding tree \mathcal{T} is as follows:

$$\mathcal{L}_{SE}^{\mathcal{T}}(\mathbf{W}) = - \sum_{j=1}^q \frac{((\mathbf{1} - \mathbf{W})^{\top} \mathbf{A} \mathbf{W})_{jj}}{\text{sum}(\mathbf{A})} \log_2 \frac{(\mathbf{1}^{\top} \mathbf{A} \mathbf{W})_{jj}}{\text{sum}(\mathbf{A})},$$

s.t. $\mathbf{W} \mathbf{1}_q = \mathbf{1}_d,$ (5)

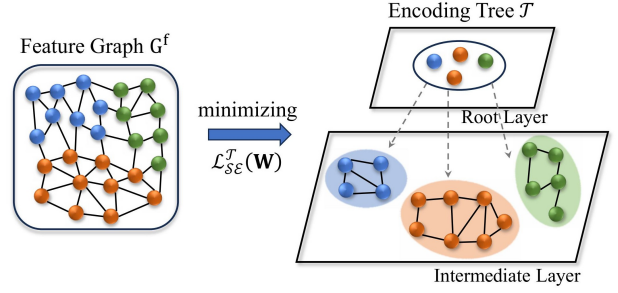


Fig. 4: Subgraphs formed by nodes of the same color are high-densely connected, which is defined as “redundancy”. By minimizing structural entropy, the feature graph G^f is converted into an optimal encoding tree \mathcal{T} , which increases intra-layer edge weights while decreasing the weights from nodes to the root of their parent layer.

where $\mathbf{1}_q$ and $\mathbf{1}_d$ are the q -dimensional and d -dimensional all-ones column vectors, respectively, $\text{sum}(\cdot)$ denotes the element-wise summation of a matrix.

“Redundancy” is characterized as high-density connected subgraphs based on the definition of the feature graph G^f . By minimizing structural entropy, the feature graph G^f is converted into an optimal encoding tree \mathcal{T} , which increases intra-layer edge weights while decreasing the weights from nodes to the root of their parent layer. Unlike mutual information-based methods, SEHFS explicitly models intra-layer and node–root correlations, achieving higher-order correlation learning. This aggregation effectively groups high-densely connected subgraphs into single nodes and amplifies inter-node edge weights, thereby eliminating redundancy. The principle of redundancy elimination in SEHFS is shown in Figure 4. The q low-redundancy feature clusters are then mapped by the classifier to q labels, resulting in more effective and low-redundancy feature selection.

B. Global View Matrix Reconstruction

In multi-view multi-label learning, information-theoretic methods are challenged in optimizing data from different views. To address this, global view matrix reconstruction is proposed to obtain a unified feature matrix with cross-view consistency, facilitating global feature selection. The reconstruction of the global view matrix mainly consists of two components: (1) learning a shared semantic matrix to capture consistency; (2) learning view-specific contribution matrices to capture complementarity. By integrating these two components, the global view matrix achieves a balance between shared consistency and unique complementarity across views.

1) *Learning Shared Semantic Matrix:* The semantic matrix of v -th view $\mathbf{S}_v \in \mathbb{R}^{n \times n}$ represents the semantics of v -th view by calculating the relationships among samples. \mathbf{S}_v is calculated as follows:

$$s_{ij}^{(v)} = \begin{cases} \exp\left(-\frac{\|x_i^{(v)} - x_j^{(v)}\|_2^2}{\sigma^2}\right) & \text{if } x_i^{(v)} \in \mathcal{N}_k(x_j^{(v)}) \text{ or} \\ & x_j^{(v)} \in \mathcal{N}_k(x_i^{(v)}) \\ 0 & \text{otherwise,} \end{cases} \quad (6)$$

where σ represents a predefined parameter, and $\mathcal{N}_k(x_j^{(v)})$ represents the set of k nearest neighbors of $x_j^{(v)}$.

The shared semantic matrix $\mathbf{S} \in \mathbb{R}^{n \times n}$ is obtained by integrating the semantic matrix \mathbf{S}_v of each view, and the similarity between \mathbf{S}_v and \mathbf{S} guides the learning of the view weight $\alpha_v \in \mathbb{R}^+$. Serving as the core component of the global view matrix $\mathbf{X}^f \in \mathbb{R}^{n \times d}$, the shared semantic matrix \mathbf{S} , together with view weight vector $\alpha \in \mathbb{R}^{V \times 1}$, directly guides the integration of each view matrix $\mathbf{X}_v \in \mathbb{R}^{n \times d(v)}$. To learn each view matrix under the global view dimensionality, a transformation matrix $\mathbf{P}_v \in \mathbb{R}^{d(v) \times d}$ is defined. When concatenating the views in sequence, \mathbf{P}_v is constructed as a diagonal matrix with all ones and a specific offset determined by the number of features $d(v)$ in each view. In this way, $\mathbf{X}_v \mathbf{P}_v \in \mathbb{R}^{n \times d}$ enables the unified integration of all views. The following objective function is formulated as the main component for global view matrix reconstruction:

$$\min_{\mathbf{X}^f, \mathbf{S}, \alpha_v} \beta \left\{ \|\mathbf{X}^f - \mathbf{S} \sum_{v=1}^V \alpha_v \mathbf{X}_v \mathbf{P}_v\|_F^2 + \|\mathbf{S} - \sum_{v=1}^V \alpha_v \mathbf{S}_v\|_F^2 \right\} + \lambda \text{Tr}(\mathbf{L}_Y^\top \mathbf{S} \mathbf{L}_Y), \quad s.t. \quad \mathbf{X}^f, \mathbf{S}, \alpha_v \geq 0, \quad (7)$$

where a graph Laplacian regularization term $\text{Tr}(\mathbf{L}_Y^\top \mathbf{S} \mathbf{L}_Y)$ is introduced to ensure consistency between the shared semantic matrix and the label matrix. Here, $\mathbf{L}_Y = \mathbf{D}_Y - \mathbf{S}_Y \in \mathbb{R}^{n \times n}$ denotes the graph Laplacian matrix of the label matrix, \mathbf{S}_Y is a sample-wise cosine similarity matrix computed from the label matrix \mathbf{Y} , and \mathbf{D}_Y is the degree matrix with diagonal elements equal to the row sums of \mathbf{S}_Y . Minimizing this regularization term effectively enhances the intrinsic correlation between features and labels, thereby improving the discriminability of feature representations.

2) *Supplementing View-specific Contribution Matrix*: To compensate for the missing view-specific information in \mathbf{S} , the view-specific contribution matrix of each view needs to be supplemented to \mathbf{X}^f . By utilizing the transpose of the transformation matrix \mathbf{P}_v^\top , \mathbf{X}^f under the dimensionality $d(v)$ of v -th view can be calculated. Accordingly, for v -th view, a unique matrix \mathbf{H}_v is learned. \mathbf{X}^f under the corresponding view dimension is encouraged to be similar to the view-specific contribution matrix $\mathbf{X}_v \mathbf{H}_v$. Together with Formula (7), the following objective function is formulated as follows:

$$\min_{\mathbf{X}^f, \mathbf{S}, \mathbf{H}_v, \alpha_v} \beta \left\{ \|\mathbf{X}^f - \mathbf{S} \sum_{v=1}^V \alpha_v \mathbf{X}_v \mathbf{P}_v\|_F^2 + \|\mathbf{S} - \sum_{v=1}^V \alpha_v \mathbf{S}_v\|_F^2 \right\} + \lambda \text{Tr}(\mathbf{L}_Y^\top \mathbf{S} \mathbf{L}_Y) + \gamma \sum_{v=1}^V \|\mathbf{X}^f \mathbf{P}_v^\top - \mathbf{X}_v \mathbf{H}_v\|_F^2, \quad s.t. \quad \mathbf{X}^f, \mathbf{S}, \mathbf{H}_v, \alpha_v \geq 0. \quad (8)$$

C. Information-Matrix Fusion Framework

To reconcile global and local objectives, we propose a novel multi-view, multi-label framework. It reconstructs a global view matrix to optimize the overall structure and, in conjunction with a structural entropy-guided feature selection module, performs sample-level optimization by selecting features from

the reconstructed global matrix. The final objective function is as follows:

$$\min_{\mathbf{X}^f, \mathbf{W}, \mathbf{S}, \mathbf{H}_v, \alpha_v} \|\mathbf{X}^f \mathbf{W} - \mathbf{Y}\|_F^2 + \alpha \mathcal{L}_{SE}^T(\mathbf{W}) + \beta \left\{ \|\mathbf{X}^f - \mathbf{S} \sum_{v=1}^V \alpha_v \mathbf{X}_v \mathbf{P}_v\|_F^2 + \|\mathbf{S} - \sum_{v=1}^V \alpha_v \mathbf{S}_v\|_F^2 \right\} + \lambda \text{Tr}(\mathbf{L}_Y^\top \mathbf{S} \mathbf{L}_Y) + \gamma \sum_{v=1}^V \|\mathbf{X}^f \mathbf{P}_v^\top - \mathbf{X}_v \mathbf{H}_v\|_F^2, \quad s.t. \quad \mathbf{X}^f, \mathbf{W}, \mathbf{S}, \mathbf{H}_v, \alpha_v \geq 0, \quad \mathbf{W} \mathbf{1}_q = \mathbf{1}_d. \quad (9)$$

D. Optimization

For the above optimization problem, an iterative optimization method is designed to solve one variable by fixing other variables. The overall objective function Formula (9) has a total of five variables $\mathbf{X}^f, \mathbf{W}, \mathbf{S}, \mathbf{H}_v, \alpha_v$ to be optimized. The optimization details of the five variables are presented as follows:

1) *Update \mathbf{X}^f, \mathbf{S} and \mathbf{H}_v* : The equivalence formula for the Frobenius norm is defined as $\|\mathbf{X}\|_F^2 = \text{Tr}(\mathbf{X}^\top \mathbf{X})$. So the objective function can be rewritten as:

$$\Theta(\mathbf{X}^f, \mathbf{S}, \mathbf{H}_v) = \text{Tr}((\mathbf{X}^f \mathbf{W} - \mathbf{Y})^\top (\mathbf{X}^f \mathbf{W} - \mathbf{Y})) + \beta \text{Tr}((\mathbf{X}^f - \mathbf{S} \sum_{v=1}^V \alpha_v \mathbf{X}_v \mathbf{P}_v)^\top (\mathbf{X}^f - \mathbf{S} \sum_{v=1}^V \alpha_v \mathbf{X}_v \mathbf{P}_v)) + \beta \text{Tr}((\mathbf{S} - \sum_{v=1}^V \alpha_v \mathbf{S}_v)^\top (\mathbf{S} - \sum_{v=1}^V \alpha_v \mathbf{S}_v)) + \lambda \text{Tr}(\mathbf{L}_Y^\top \mathbf{S} \mathbf{L}_Y) + \gamma \sum_{v=1}^V \text{Tr}((\mathbf{X}^f \mathbf{P}_v^\top - \mathbf{X}_v \mathbf{H}_v)^\top (\mathbf{X}^f \mathbf{P}_v^\top - \mathbf{X}_v \mathbf{H}_v)). \quad (10)$$

Multiplicative gradient descent strategy [44] is adopted to solve Eq. (10). Meanwhile, to maintain the validity of the constraints, the following update rules are derived according to the KKT conditions:

$$\mathbf{X}^f \leftarrow \mathbf{X}^f \cdot \frac{\mathbf{Y} \mathbf{W}^\top + \sum_{v=1}^V \beta \alpha_v \mathbf{S} \mathbf{X}_v \mathbf{P}_v + \gamma \mathbf{X}_v \mathbf{H}_v \mathbf{P}_v}{\mathbf{X}^f \mathbf{W} \mathbf{W}^\top + \beta \mathbf{X}^f + \gamma \sum_{v=1}^V \mathbf{X}^f \mathbf{P}_v^\top \mathbf{P}_v}, \quad (11)$$

$$\mathbf{S} \leftarrow \mathbf{S} \cdot \frac{\beta \mathbf{X}^f \sum_{v=1}^V \alpha_v \mathbf{P}_v^\top \mathbf{X}_v^\top + \beta \sum_{v=1}^V \alpha_v \mathbf{S}_v}{\beta \mathbf{S} \sum_{v=1}^V \alpha_v^2 \mathbf{X}_v \mathbf{P}_v \mathbf{P}_v^\top \mathbf{X}_v^\top + (\lambda \mathbf{L}_Y \mathbf{L}_Y^\top + \beta \mathbf{I}) \mathbf{S}}, \quad (12)$$

$$\mathbf{H}_v \leftarrow \mathbf{H}_v \cdot \frac{\mathbf{X}_v^\top \mathbf{X}^f \mathbf{P}_v^\top}{\mathbf{X}_v^\top \mathbf{X}_v \mathbf{H}_v}. \quad (13)$$

When implementing the optimization, a small positive value $\varepsilon \rightarrow 0^+$ is added to the denominator to prevent division-by-zero errors.

2) *Update \mathbf{W}* : Given $\mathbf{X}^f \in \mathbb{R}^{n \times d}$, $\mathbf{Y} \in \mathbb{R}^{n \times r}$, and a fixed matrix $\mathbf{A} \in \mathbb{R}^{d \times d}$, we estimate $\mathbf{W} \in \mathbb{R}^{d \times r}$ by

$$\min_{\mathbf{W}} J(\mathbf{W}) = \|\mathbf{X}^f \mathbf{W} - \mathbf{Y}\|_F^2 + \alpha \mathcal{L}_{SE}^T(\mathbf{W}), \quad s.t. \quad \mathbf{W} \geq \mathbf{0}, \quad \mathbf{W} \mathbf{1}_q = \mathbf{1}_d. \quad (14)$$

Algorithm 1 Pseudo code of SEHFS

Input: Data matrices $\{\mathbf{X}_v\}_{v=1}^V$; Label matrix \mathbf{Y} .

Parameter: Hyperparameters $\alpha, \beta, \gamma, \lambda$.

Output: Selected features fea_idx .

- 1: Initialize $\mathbf{X}^f, \mathbf{W}, \mathbf{H}_v, \alpha_v$;
- 2: **for** $v = 1$ to V **do**
- 3: Calculate \mathbf{S}_v by Eq. (6);
- 4: **end for**
- 5: Calculate $\mathbf{L}_Y = \mathbf{D}_Y - \mathbf{S}_Y$;
- 6: Calculate the mutual information matrix \mathbf{A} ;
- 7: **while** not converged **do**
- 8: Update \mathbf{X}^f by Eq. (11);
- 9: Update \mathbf{W} by Eq. (17);
- 10: Update \mathbf{S} by Eq. (12);
- 11: Update \mathbf{H}_v by Eq. (13);
- 12: Update α_v by Formula (22);
- 13: **end while**
- 14: **return** fea_idx according to $\|\mathbf{W}_i\|_2$.

Setting $S = \text{sum}(\mathbf{A}) = \sum_{i=1}^d \sum_{k=1}^d \mathbf{A}_{ik} = \mathbf{1}^\top \mathbf{A} \mathbf{1}$, $\mathbf{q}_j = \mathbf{1}^\top \mathbf{A} \mathbf{w}_j$, $\mathbf{g}_j = (\mathbf{1} - \mathbf{w}_j)^\top \mathbf{A} \mathbf{w}_j$, where $\mathbf{1} \in \mathbb{R}^d$ denote the all-ones vector, \mathbf{w}_j represents the j -th column of \mathbf{W} , thus the optimization subproblem Eq. (14) is transformed into:

$$\mathcal{L}_{SE}^T(W) = -\frac{1}{S} \sum_{j=1}^q g_j \log_2 \left(\frac{q_j}{S} \right). \quad (15)$$

In implementation, a small positive value $\varepsilon \rightarrow 0^+$ is used to guard the logarithm, i.e., $q_j \leftarrow \max(q_j, \varepsilon)$. The gradients can be expressed as follows:

$$\begin{aligned} \nabla_{\mathbf{W}} \|\mathbf{X}^f \mathbf{W} - \mathbf{Y}\|_F^2 &= 2 \mathbf{X}^f{}^\top (\mathbf{X}^f \mathbf{W} - \mathbf{Y}), \\ \nabla_{\mathbf{w}_j} \mathcal{L}_{SE}^T &= -\frac{1}{S} \left[h_j (\mathbf{a} - \mathbf{A}_{\text{sym}} \mathbf{w}_j) + \frac{g_j}{\ln 2 q_j} \mathbf{a} \right], \end{aligned} \quad (16)$$

where h_j denotes $\log_2 \left(\frac{q_j}{S} \right)$, \mathbf{a} denotes $\mathbf{A}^\top \mathbf{1}$, and \mathbf{A}_{sym} denotes $\mathbf{A} + \mathbf{A}^\top$. Thus, the optimization subproblem is then solved using the projected gradient descent method:

$$\begin{aligned} \mathbf{G}_W^{(t)} &= \nabla_{\mathbf{W}} J(\mathbf{W}^{(t)}), \\ \widetilde{\mathbf{W}} &= \mathbf{W}^{(t)} - \eta_t \mathbf{G}_W^{(t)}, \\ \mathbf{W}^{(t+1)} &= \Pi_{\Delta}(\widetilde{\mathbf{W}}), \end{aligned} \quad (17)$$

where Π_{Δ} projects each row onto the probability simplex $\Delta = \{\mathbf{w} \in \mathbb{R}^r : \mathbf{w} \geq \mathbf{0}, \mathbf{1}^\top \mathbf{w} = 1\}$. The row-wise projection [45] is given by

$$\begin{aligned} \mathbf{u} &= \text{sort}(\mathbf{v}) \text{ (desc.)}, \quad c_k = \sum_{i=1}^k u_i, \\ \rho &= \max\{k : u_k - \frac{c_k - 1}{k} > 0\}, \\ \theta &= \frac{c_\rho - 1}{\rho}, \\ [\Pi_{\Delta}(\mathbf{v})]_i &= \max\{v_i - \theta, 0\}. \end{aligned} \quad (18)$$

The step size η_t is chosen by Armijo backtracking until

$$J(\Pi_{\Delta}(\mathbf{W}^{(t)} - \eta_t \mathbf{G}_W^{(t)})) \leq J(\mathbf{W}^{(t)}) - c \eta_t \|\mathbf{G}_W^{(t)}\|_F^2, \quad (19)$$

and the iteration stops when the relative decrease satisfies

$$\frac{|J(\mathbf{W}^{(t+1)}) - J(\mathbf{W}^{(t)})|}{J(\mathbf{W}^{(t)}) + \varepsilon} < \tau. \quad (20)$$

3) *Update α_v* : By fixing other variables, the optimization subproblem for α_v can be written as follows:

$$\min_{\alpha_v} \|\mathbf{X}^f - \mathbf{S} \sum_{v=1}^V \alpha_v \mathbf{X}_v \mathbf{P}_v\|_F^2 + \|\mathbf{S} - \sum_{v=1}^V \alpha_v \mathbf{S}_v\|_F^2. \quad (21)$$

Setting $\psi = \text{vec}(\mathbf{X}^f) \in \mathbb{R}^{nd \times 1}$, $\Psi = \text{vec}([\mathbf{S} \mathbf{X}_1 \mathbf{P}_1, \dots, \mathbf{S} \mathbf{X}_V \mathbf{P}_V]) \in \mathbb{R}^{nd \times V}$, and likewise, $\omega = \text{vec}(\mathbf{S}) \in \mathbb{R}^{nn \times 1}$, $\Omega = \text{vec}([\mathbf{S}_1, \dots, \mathbf{S}_V]) \in \mathbb{R}^{nn \times V}$, thus the optimization Subproblem 21 is transformed into:

$$\min_{\alpha_v} \alpha^\top \mathbf{M} \alpha - \alpha^\top \mathbf{h}, \quad (22)$$

where $\mathbf{M} = \Psi^\top \Psi + \Omega^\top \Omega$, $\mathbf{h} = 2(\Psi^\top \psi + \Omega^\top \omega)$. Due to the semi-definite \mathbf{M} , Formula (22) is a quadratic convex programming problem and can be solved efficiently [46].

E. Complexity Analysis

We analyze the time complexity of SEHFS. Let n denote the number of samples, $d = \sum_{v=1}^V d(v)$ the total feature dimension across all V views, and q the number of labels. The primary cost stems from five per-iteration components in the alternating optimization procedure (Algorithm 1), preceded by a one-time initialization.

a) *Initialization*: Constructing the semantic matrices $\{\mathbf{S}_v\}_{v=1}^V$ and the mutual information matrix \mathbf{A} requires pairwise similarity or information-theoretic computations. Computing \mathbf{S}_v via k -nearest neighbors for a single view costs $\mathcal{O}(n^2 d(v))$, totaling $\mathcal{O}(n^2 d)$ over all views. Building the $d \times d$ mutual information matrix \mathbf{A} by evaluating pairwise MI among features costs $\mathcal{O}(nd^2)$. These operations are performed once before iterations.

TABLE I: The detailed information for the datasets in our experiment

Datasets	EMOTIONS	YEAST	VOC07	MIRFlickr	SCENE	OBJECT	Corel5K	IAPRTC12
View-1(d_1)	Rhythmic(8)	GE(79)	DH(100)	DH(100)	CH(64)	CH(64)	DH(100)	DH(100)
View-2(d_2)	Timbre(64)	PP(24)	GIST(512)	GIST(512)	CM(225)	CM(225)	DHV3H1(300)	DHV3H1(300)
View-3(d_3)	-	-	HH(100)	HH(100)	CORR(144)	CORR(144)	GIST(512)	GIST(512)
View-4(d_4)	-	-	-	-	EDH(73)	EDH(73)	HHV3H1(300)	HHV3H1(300)
View-5(d_5)	-	-	-	-	WT(128)	WT(128)	HH(100)	HH(100)
Instances(n)	593	2417	3817	4053	4400	6047	4999	4999
Features(d)	72	103	712	712	634	634	1312	1312
Labels(q)	6	12	20	38	33	31	260	260

TABLE II: Experimental results \uparrow (mean \pm std) of each method on AP(%); the best result is shown in bold and the second-best is underlined.

Datasets	SEHFS	DHLI	GRAFS	MSFS	MIFS	SPLDG	SRFS	MSSL
EMOTIONS	.686\pm.052	.591 \pm .045	.605 \pm .036	.591 \pm .050	.637 \pm .049	.654 \pm .049	.666 \pm .052	.631 \pm .048
YEAST	<u>.670\pm.019</u>	.663 \pm .022	.665 \pm .020	.651 \pm .039	.663 \pm .024	.663 \pm .019	.672\pm.021	.660 \pm .020
VOC07	<u>.592\pm.019</u>	.585 \pm .017	.586 \pm .020	<u>.593\pm.016</u>	.576 \pm .021	.583 \pm .015	.598\pm.016	.577 \pm .016
MIRFlickr	.692\pm.022	.655 \pm .016	.659 \pm .025	.682 \pm .019	.646 \pm .019	.682 \pm .015	<u>.687\pm.019</u>	.678 \pm .020
SCENE	.804\pm.019	.786 \pm .018	.801 \pm .019	.718 \pm .046	.792 \pm .017	.788 \pm .017	<u>.801\pm.016</u>	.797 \pm .018
OBJECT	.454\pm.052	.408 \pm .051	<u>.437\pm.056</u>	.357 \pm .049	.436 \pm .044	.423 \pm .050	<u>.435\pm.045</u>	.433 \pm .054
Corel5K	.210\pm.039	.191 \pm .040	<u>.196\pm.039</u>	.184 \pm .035	.157 \pm .032	.173 \pm .040	.177 \pm .039	.190 \pm .036
IAPRTC12	.215\pm.015	.192 \pm .015	<u>.193\pm.017</u>	.184 \pm .017	.175 \pm .018	.183 \pm .018	.182 \pm .017	.190 \pm .017

TABLE III: Experimental results \downarrow (mean \pm std) of each method on Cov(%); the best result is shown in bold and the second-best is underlined.

Datasets	SEHFS	DHLI	GRAFS	MSFS	MIFS	SPLDG	SRFS	MSSL
EMOTIONS	.663\pm.029	.775 \pm .035	.749 \pm .029	.769 \pm .033	.722 \pm .031	.706 \pm .033	<u>.681\pm.026</u>	.721 \pm .033
YEAST	<u>.679\pm.034</u>	.690 \pm .037	.682 \pm .034	.729 \pm .062	<u>.679\pm.042</u>	.688 \pm .039	.675\pm.035	.689 \pm .034
VOC07	.441\pm.005	.458 \pm .005	.459 \pm .006	.454 \pm .004	<u>.495\pm.006</u>	.454 \pm .004	<u>.445\pm.004</u>	.474 \pm .005
MIRFlickr	.582\pm.007	.635 \pm .007	.617 \pm .011	.592 \pm .006	.640 \pm .007	<u>.585\pm.005</u>	<u>.587\pm.006</u>	.592 \pm .006
SCENE	.430\pm.009	.456 \pm .008	.439 \pm .008	.499 \pm .010	.448 \pm .008	<u>.457\pm.009</u>	<u>.435\pm.008</u>	.446 \pm .009
OBJECT	.311\pm.010	.338 \pm .008	<u>.319\pm.009</u>	.375 \pm .008	.320 \pm .009	.331 \pm .008	<u>.323\pm.007</u>	.334 \pm .009
Corel5K	.491\pm.018	.516 \pm .018	<u>.515\pm.019</u>	.527 \pm .017	.571 \pm .015	.553 \pm .017	.545 \pm .017	.539 \pm .017
IAPRTC12	.409\pm.012	<u>.427\pm.012</u>	<u>.428\pm.012</u>	.462 \pm .016	.511 \pm .011	.458 \pm .015	.474 \pm .015	.432 \pm .012

TABLE IV: Experimental results \downarrow (mean \pm std) of each method on HL(%); the best result is shown in bold and the second-best is underlined.

Datasets	SEHFS	DHLI	GRAFS	MSFS	MIFS	SPLDG	SRFS	MSSL
EMOTIONS	.246\pm.031	.297 \pm .032	.297 \pm .031	.332 \pm .059	.275 \pm .031	.271 \pm .032	.255 \pm .028	.274 \pm .039
YEAST	.223\pm.007	.225 \pm .009	.230 \pm .007	.254 \pm .013	.224 \pm .009	.230 \pm .008	<u>.223\pm.009</u>	.230 \pm .008
VOC07	.079\pm.004	.085 \pm .004	.085 \pm .005	.087 \pm .005	.085 \pm .004	<u>.084\pm.004</u>	<u>.084\pm.004</u>	.086 \pm .004
MIRFlickr	.167\pm.010	.189 \pm .007	.184 \pm .010	.175 \pm .009	.188 \pm .007	<u>.173\pm.007</u>	<u>.172\pm.009</u>	.176 \pm .009
SCENE	.092\pm.007	.103 \pm .008	.098 \pm .007	.136 \pm .019	.102 \pm .006	.100 \pm .006	<u>.097\pm.007</u>	.099 \pm .006
OBJECT	.052\pm.005	.059 \pm .004	.057 \pm .004	.069 \pm .004	.060 \pm .005	.057 \pm .004	<u>.056\pm.004</u>	.057 \pm .004
Corel5K	.013\pm.001	.014 \pm .001	.014 \pm .001	.015 \pm .001	<u>.013\pm.001</u>	.014 \pm .001	<u>.014\pm.001</u>	.014 \pm .001
IAPRTC12	.017\pm.002	.018 \pm .002	.018 \pm .002	.019 \pm .002	<u>.018\pm.002</u>	.018 \pm .002	.018 \pm .002	.018 \pm .002

TABLE V: Experimental results \downarrow (mean \pm std) of each method on RL(%); the best result is shown in bold and the second-best is underlined.

Datasets	SEHFS	DHLI	GRAFS	MSFS	MIFS	SPLDG	SRFS	MSSL
EMOTIONS	.272\pm.051	.383 \pm .056	.362 \pm .043	.395 \pm .062	.330 \pm .054	.316 \pm .053	<u>.291\pm.047</u>	.333 \pm .057
YEAST	<u>.249\pm.015</u>	.255 \pm .018	.254 \pm .015	.278 \pm .038	.254 \pm .019	.256 \pm .015	.247\pm.016	.259 \pm .016
VOC07	.194\pm.017	.206 \pm .015	.206 \pm .019	.204 \pm .014	.225 \pm .018	.205 \pm .013	<u>.194\pm.014</u>	.215 \pm .014
MIRFlickr	.149\pm.014	.180 \pm .010	.173 \pm .017	.159 \pm .013	.183 \pm .011	.156 \pm .009	<u>.154\pm.012</u>	.159 \pm .012
SCENE	.085\pm.011	.099 \pm .011	.091 \pm .011	.136 \pm .025	.097 \pm .011	.100 \pm .011	<u>.090\pm.010</u>	.093 \pm .011
OBJECT	.173\pm.027	.199 \pm .025	<u>.182\pm.027</u>	.228 \pm .025	.183 \pm .024	.192 \pm .024	<u>.186\pm.022</u>	.185 \pm .026
Corel5K	.234\pm.043	.249 \pm .044	<u>.247\pm.045</u>	.257 \pm .044	.292 \pm .047	.279 \pm .051	.272 \pm .049	.254 \pm .044
IAPRTC12	.167\pm.015	<u>.178\pm.017</u>	.179 \pm .015	.199 \pm .025	.223 \pm .017	.196 \pm .025	.206 \pm .025	.183 \pm .017

b) *Iterative updates:* Updating the global view matrix \mathbf{X}^f (Eq. (11)) involves multiplications of size $n \times n$ and $n \times d$, yielding a per-iteration cost of $\mathcal{O}(n^2d)$. Updating the shared semantic matrix \mathbf{S} (Eq. (12)) operates on $n \times d$ matrices and, with precomputation, costs $\mathcal{O}(n^2d)$ per iteration. Updating the assignment matrix \mathbf{W} (Eq. (17)) requires gradients for the structural entropy term and reconstruction loss; the structural-entropy gradient uses $\mathbf{X}^f \in \mathbb{R}^{n \times d}$ and $\mathbf{W} \in \mathbb{R}^{d \times q}$, costing $\mathcal{O}(ndq)$ per iteration. In the v -th view, updating \mathbf{H}_v is dominated by matrix operations with complexity $\mathcal{O}(nd^2)$, while updating α_v is dominated by solving a quadratic program with complexity $\mathcal{O}(n^2)$.

c) *Overall complexity:* Assuming convergence in T iterations, the total time complexity is $\mathcal{O}(T(n^2d + nd^2))$, scaling

linearly with T and polynomially with n and d .

IV. EXPERIMENTS

A. Datasets

Our method is evaluated on eight widely used multi-view multi-label datasets from different domains: EMOTIONS [47] for image sentiment analysis, YEAST [48] for gene function prediction, VOC07 [49] for image classification, MIRFlickr [50] for multimedia annotation, SCENE [51] and OBJECT [51] for image retrieval, Corel5K [52] and IAPRTC12 [53] for image annotation. The datasets contain varying numbers of views, ranging from 2 to 5, and the number of features per view also varies from tens to thousands. The

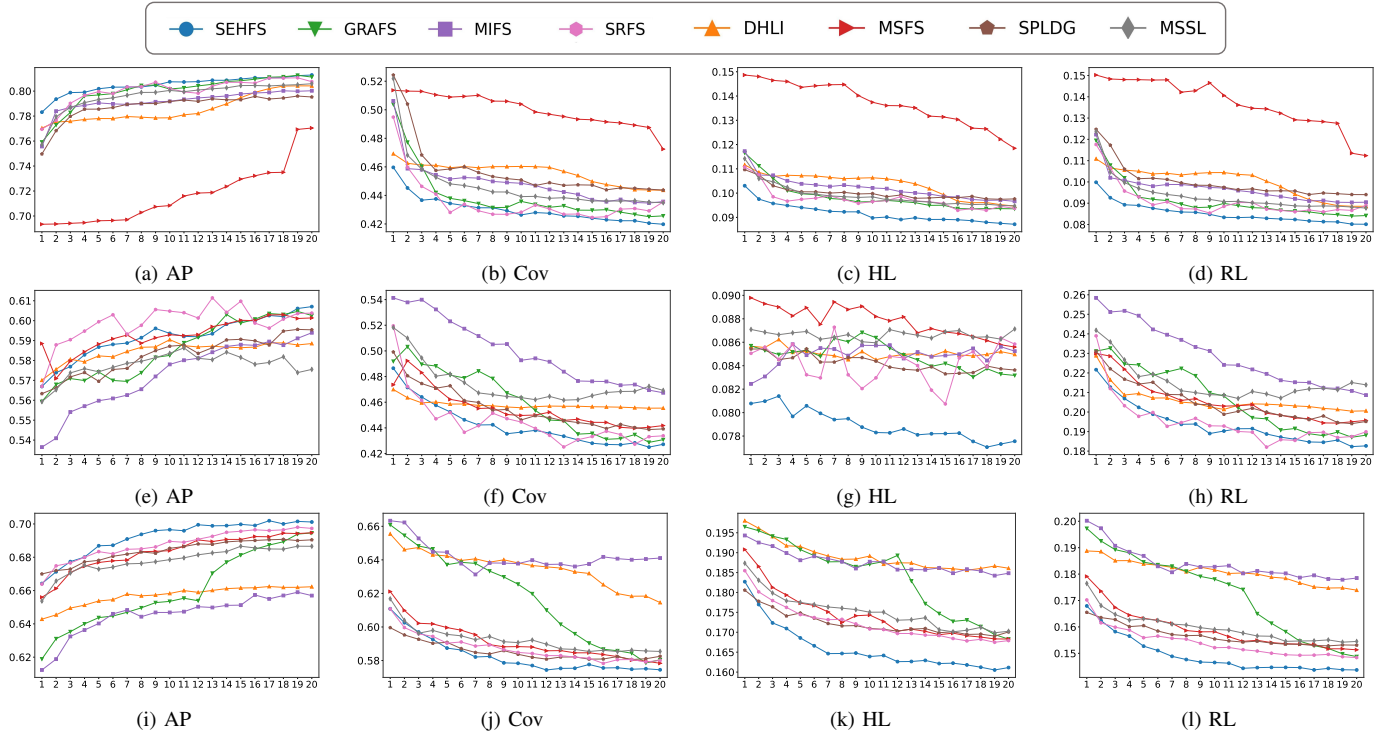


Fig. 5: Performance comparison of SEHFS and seven baseline methods on SCENE (first row), VOC07 (second row), and MIRFlickr (third row). The horizontal axis denotes the number of selected features and the vertical axis reports AP, Cov, HL, and RL.



Fig. 6: Comparison of SEHFS with other methods using the Bonferroni-Dunn test. Methods not connected to SEHFS indicate a significant difference in performance (CD = 3.2946 at the significance level of 0.05).

dataset details are presented in Table I, where ‘-’ is used to denote the absence of the corresponding view in the dataset.

B. Experimental setup

a) *Evaluation Metrics*: Four widely used multi-view multi-label evaluation metrics are adopted: Average Precision (AP), Coverage (Cov), Hamming Loss (HL), and Ranking Loss (RL). For AP, larger values indicate better performance and are denoted by \uparrow in the table. For Cov, HL, and RL, smaller values indicate better performance and are denoted by \downarrow in the table.

b) *Baselines*: Seven state-of-the-art methods are introduced as baselines in the experiments: three multi-view multi-label feature selection methods (DHLI [36], GRAFS [37], MSFS [40]) and four multi-label feature selection methods (SRFS [27], SPLDG [25], MSSL [24], MIFS [23]). The top 20% of features are uniformly selected for comparison using the MLkNN classifier [54]. Results are presented as mean evaluation scores with standard deviations obtained by ten-fold cross-validation. The parameters for each method are tuned within the range of $\{10^{-3}, 10^{-2}, \dots, 10^3\}$ to ensure a fair and valid comparison.

C. Experimental result

The detailed results for AP, Cov, HL, and RL are presented in Table II, III, IV and V, where the mean results and standard deviations are recorded. According to the 256 statistical comparisons, some key observations are clearly revealed:

- Among four evaluation metrics across all eight datasets, the proposed method SEHFS achieved the best evaluation in 87.5% of cases. Among the remaining cases, all are ranked second-best except for the AP metric on VOC07. Regarding the HL metric specifically, SEHFS achieved the best evaluation with a perfect 100% rate. This indicates that minimizing the structural entropy regularization term learns high-order feature correlations and directly selects more suitable and low-redundancy feature support for each label.
- Among all baselines, SEHFS is observed to outperform the three multi-view multi-label methods across all metrics on all datasets, except on the AP metric for VOC07. On YEAST and VOC07, which have fewer views and smaller scale, no advantage over the multi-label learning methods SPLDG and SRFS is observed. In contrast, on SCENE, OBJECT, Corel5K, and IAPRTC12, which have more views and larger scale, SEHFS achieves the best

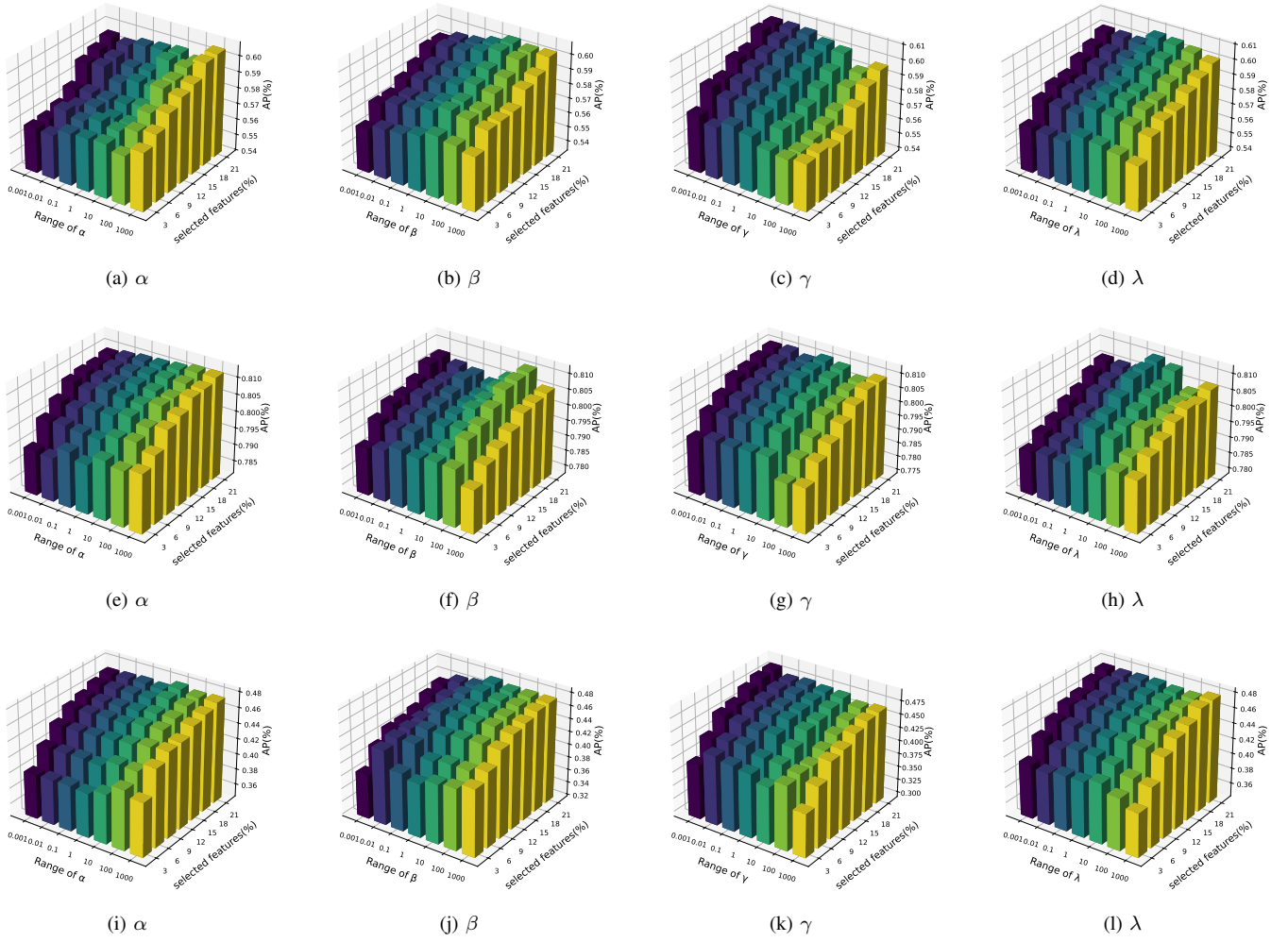


Fig. 7: Parameter sensitivity analysis of SEHFS on VOC07 (first row), SCENE (second row), and OBJECT (third row), where the horizontal axis indicates the parameter range, the vertical axis shows the number of selected features, and the depth axis represents AP.

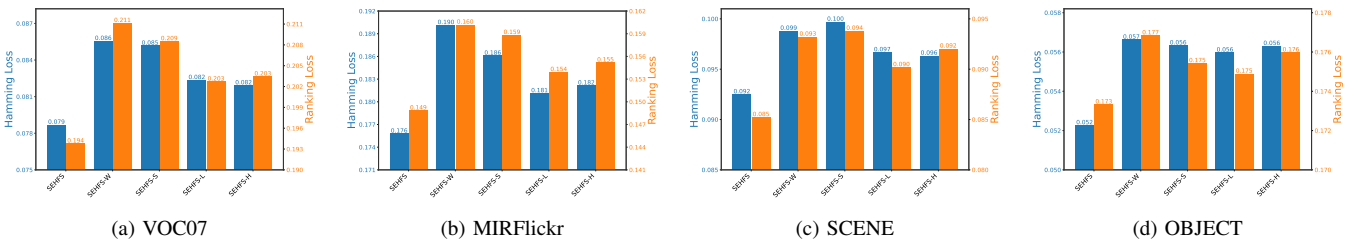


Fig. 8: Ablation study results of SEHFS on VOC07, MIRFlickr, SCENE, and OBJECT, where each subfigure lists SEHFS and its four variants on the horizontal axis and reports the evaluation metric on the vertical axis, with HL on the left and RL on the right.

performance across all metrics and outperforms all seven baselines. These results demonstrate the effectiveness of SEHFS for multi-view learning. Moreover, on these four larger datasets, SEHFS exceeds the best results of baselines by 7.24% on average, indicating that the structural entropy regularization term effectively learns high-order feature correlations from more complex data structures and provides robustness to noise.

- A more intuitive comparison among all eight methods on SCENE at different percentages of selected features is presented in Figure 5. As the proportion of selected

features increases, the superiority of SEHFS and the effectiveness of feature selection are clearly observed.

The Friedman test [55] is employed on all four metrics to evaluate the relative performance of the baselines, and Table VI reports the Friedman statistic F_F for each metric together with the corresponding critical value. From Table VI, it is evident that the null hypothesis, which assumes no difference in model performance between the methods, is rejected at the significance level ($\alpha = 0.05$). Consequently, a significant difference between the methods is indicated.

Following the rejection of the null hypothesis in the Fried-

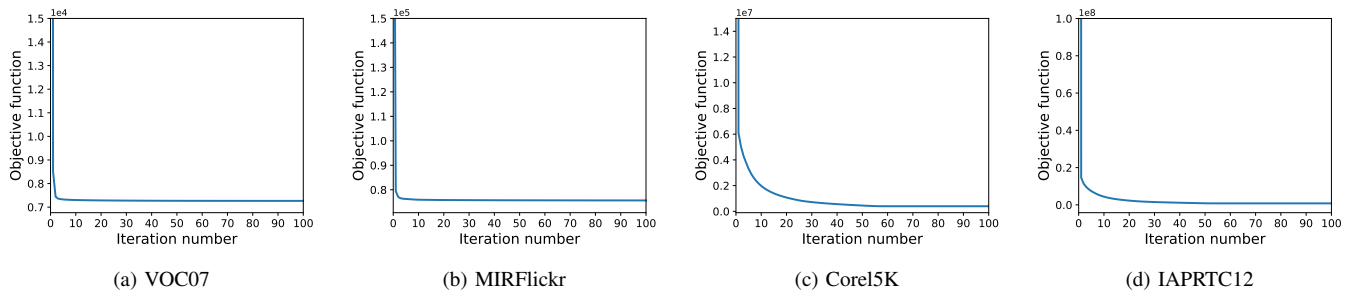


Fig. 9: Convergence curve of SEHFS on VOC07, MIRFlickr, Corel5K, and IAPRTC12.

TABLE VI: Friedman statistics F_F over four evaluation metrics, along with the critical value at a 0.05 significance level for SEHFS.

Evaluation Metric	F_F	Critical value
Average Precision	6.0485	2.2032
Coverage Error	5.9945	
Hamming Loss	16.5200	
Ranking Loss	5.8174	

man test, the Bonferroni-Dunn test [55], a non-parametric statistical hypothesis testing method, is employed for pairwise comparisons. The critical value $q_\alpha = 2.949$ and the Critical Distance $CD = 3.2946$ can be calculated at a significance level of $\alpha = 0.05$. If the difference between the average ranks of two methods is greater than CD , it indicates a significant difference in their performance. The results of this test are presented in Figure 6, from which it can be inferred that SEHFS outperforms all baselines across all four metrics.

D. Parameter analysis

SEHFS comprises four parameters: $\alpha, \beta, \gamma, \lambda$. The influence of each parameter on the performance of SEHFS in terms of the AP metric on VOC07, SCENE, and OBJECT is presented in Figure 7. In the figure, the X-axis represents the range of parameters, and the Y-axis represents the percentage of selected features. The results show that SEHFS exhibits low sensitivity to these parameters and that performance remains stable when the proportion of selected features ranges from 3% to 21%.

Furthermore, when the weight parameter α of the structural entropy regularization term is increased, SEHFS attains improved performance, as shown in the first column of Figure 7. This indicates that the structural entropy regularization term effectively learns high-order feature correlations and that its guidance aligns closely with the optimization objective.

E. Ablation study

To demonstrate the effectiveness of the structural entropy regularization term and the necessity of learning both the shared semantic matrix and the view-specific contribution matrix, four variants of the original method are designed: (1) SEHFS-W removes the structural entropy regularization term and directly learns the feature selection matrix \mathbf{W} from the classifier; (2) SEHFS-S discards learning the shared semantic matrix and reconstructs the global view matrix solely via the

view-specific contribution matrix of each view; (3) SEHFS-L removes the graph Laplacian regularization term, thereby ignoring the relationship between the shared semantic matrix and the label matrix; (4) SEHFS-H ignores the view-specific contribution matrix and learns only the shared semantic matrix to reconstruct the global view matrix. The ablation study adopts HL and RL as evaluation metrics on VOC07, MIR-Flickr, SCENE, and OBJECT, and the results are presented in Figure 8.

As shown in the figure, for HL, SEHFS-W exhibits an average degradation of 9.72% relative to the original method SEHFS, while SEHFS-L degrades by 6.17%, underscoring the effectiveness and necessity of the structural-entropy and graph-Laplacian regularizers. Moreover, both SEHFS-S and SEHFS-H underperform the original (by 9.30% and 6.76% on average, respectively), with SEHFS-S worse than SEHFS-H. This gap suggests that the shared semantic matrix is the core component of the global view matrix and contributes more than the view-specific matrix. Overall, these findings support the proposed multi-view, multi-label learning framework, in which consistency is primary and complementarity is supplementary.

F. Convergence Analysis

To further demonstrate the convergence property of SEHFS, we also implement experiments on four datasets, VOC07, MIRFlickr, Corel5K, and IAPRTC12. Figure 9 shows the objective value curves for Algorithm 1 on four datasets. From each subfigure of Figure 9, it is seen that the objective function of SEHFS shows a consistent pattern of continuous decrease and reaches stability. Moreover, our method can generally achieve rapid convergence within little iterations.

V. CONCLUSION

In this paper, we tackle the challenges brought by the large-scale MVML data with complex and diverse feature structures, proposing a novel feature selection method (SEHFS). This method employs structural entropy as a new measure for learning high-order nonlinear feature correlations and reducing redundancy, while fusing information theory and matrix operations to balance global-local generalization. Moreover, SEHFS reconstructs a global view matrix with a shared semantic matrix and view-specific contribution matrices to achieve a balance between consistency and complementarity among views. Extensive experimental results demonstrate the

superiority of our method. In the future, we plan to explore methods for handling incomplete views and noisy labels to further enhance the generalization capability of our method.

REFERENCES

- [1] J. Huang, Z.-M. Chen, Z.-M. Chen, X. Zhang, X. Zhang, Y. Ge, Y. Ge, L. Ye, L. Ye, G. Zhang *et al.*, “Label decoupling and reconstruction: A two-stage training framework for long-tailed multi-label medical image recognition,” in *Proceedings of the 32nd ACM International Conference on Multimedia*, 2024, pp. 2861–2869.
- [2] A. K. Aksoy, M. Ravanbakhsh, and B. Demir, “Multi-label noise robust collaborative learning for remote sensing image classification,” *IEEE Transactions on Neural Networks and Learning Systems*, vol. 35, no. 5, pp. 6438–6451, 2024.
- [3] Z. Yu, Z. Dong, C. Yu, K. Yang, Z. Fan, and C. P. Chen, “A review on multi-view learning,” *Frontiers of Computer Science*, vol. 19, no. 7, p. 197334, 2025.
- [4] J. Xie, M. Wang, P. W. Grant, and W. Pedrycz, “Feature selection with discernibility and independence criteria,” *IEEE Transactions on Knowledge and Data Engineering*, vol. 36, no. 11, pp. 6195–6209, 2024.
- [5] C. Zhu, D. Miao, Z. Wang, R. Zhou, L. Wei, and X. Zhang, “Global and local multi-view multi-label learning,” *Neurocomputing*, vol. 371, pp. 67–77, 2020.
- [6] Y. Lin, H. Liu, H. Zhao, Q. Hu, X. Zhu, and X. Wu, “Hierarchical feature selection based on label distribution learning,” *IEEE Transactions on Knowledge and Data Engineering*, vol. 35, no. 6, pp. 5964–5976, 2022.
- [7] C. Zhang, Z. Yu, Q. Hu, P. Zhu, X. Liu, and X. Wang, “Latent semantic aware multi-view multi-label classification,” in *Proceedings of the AAAI conference on artificial intelligence*, vol. 32, no. 1, 2018.
- [8] W. Liu, J. Yuan, G. Lyu, and S. Feng, “Label driven latent subspace learning for multi-view multi-label classification,” *Applied Intelligence*, vol. 53, no. 4, pp. 3850–3863, 2023.
- [9] Q. Han, L. Hu, and W. Gao, “Feature relevance and redundancy coefficients for multi-view multi-label feature selection,” *Information Sciences*, vol. 652, p. 119747, 2024.
- [10] G. Lyu, X. Deng, Y. Wu, and S. Feng, “Beyond shared subspace: A view-specific fusion for multi-view multi-label learning,” in *Proceedings of the AAAI conference on artificial intelligence*, vol. 36, no. 7, 2022, pp. 7647–7654.
- [11] P. Hao, W. Gao, and L. Hu, “Embedded feature fusion for multi-view multi-label feature selection,” *Pattern Recognition*, vol. 157, p. 110888, 2025.
- [12] P. Hao, W. Ding, W. Gao, and J. He, “Exploring view-specific label relationships for multi-view multi-label feature selection,” *Information Sciences*, vol. 681, p. 121215, 2024.
- [13] Y. Fan, J. Liu, J. Tang, P. Liu, Y. Lin, and Y. Du, “Learning correlation information for multi-label feature selection,” *Pattern Recognition*, vol. 145, p. 109899, 2024.
- [14] J. Dai, W. Chen, and Y. Qian, “Multi-label feature selection with missing features via implicit label replenishment and positive correlation feature recovery,” *IEEE Transactions on Knowledge and Data Engineering*, 2025.
- [15] X. Tan, C. Zhao, C. Liu, J. Wen, and Z. Tang, “A two-stage information extraction network for incomplete multi-view multi-label classification,” in *Proceedings of the AAAI conference on artificial intelligence*, vol. 38, no. 14, 2024, pp. 15 249–15 257.
- [16] L. Ma, L. Hu, Y. Li, W. Ding, and W. Gao, “Mi-mcf: A mutual information-based multilabel causal feature selection,” *IEEE Transactions on Neural Networks and Learning Systems*, 2025.
- [17] T. Yang, C. Wang, Y. Chen, and T. Deng, “A robust multi-label feature selection based on label significance and fuzzy entropy,” *International Journal of Approximate Reasoning*, vol. 176, p. 109310, 2025.
- [18] W. Gao, P. Hao, Y. Wu, and P. Zhang, “A unified low-order information-theoretic feature selection framework for multi-label learning,” *Pattern Recognition*, vol. 134, p. 109111, 2023.
- [19] A. Li and Y. Pan, “Structural information and dynamical complexity of networks,” *IEEE Transactions on Information Theory*, vol. 62, no. 6, pp. 3290–3339, 2016.
- [20] J. Bogatinovski, L. Todorovski, S. Džeroski, and D. Kocev, “Comprehensive comparative study of multi-label classification methods,” *arXiv preprint arXiv:2102.07113*, 2021.
- [21] J. Yin and W. Zhang, “Multi-view multi-label learning with double orders manifold preserving,” *Applied Intelligence*, vol. 53, no. 12, pp. 14 703–14 716, 2023.
- [22] Y. Wang, C. Wang, T. Deng, and W. Li, “Multi-label feature selection via nonlinear mapping and manifold regularization,” *Information Sciences*, vol. 704, p. 121965, 2025.
- [23] L. Jian, J. Li, K. Shu, and H. Liu, “Multi-label informed feature selection,” in *IJCAI*, vol. 16, 2016, pp. 1627–33.
- [24] Z. Cai and W. Zhu, “Multi-label feature selection via feature manifold learning and sparsity regularization,” *International journal of machine learning and cybernetics*, vol. 9, no. 8, pp. 1321–1334, 2018.
- [25] Y. Zhang, J. Tang, Z. Cao, and H. Chen, “Sparse multi-label feature selection via pseudo-label learning and dynamic graph constraints,” *Information Fusion*, vol. 118, p. 102975, 2025.
- [26] Y. Li, L. Hu, and W. Gao, “Multi-label feature selection via robust flexible sparse regularization,” *Pattern Recognition*, vol. 134, p. 109074, 2023.
- [27] Y. Li, X. Wang, X. Yang, W. Gao, W. Ding, and T. Li, “Fusion-enhanced multi-label feature selection with sparse supplementation,” *Information Fusion*, vol. 117, p. 102813, 2025.
- [28] W. Qian, J. Huang, Y. Wang, and W. Shu, “Mutual information-based label distribution feature selection for multi-label learning,” *Knowledge-Based Systems*, vol. 195, p. 105684, 2020.
- [29] J. Dai, Q. Wu, and W. Pedrycz, “Noise-resistant commonality and individuality label learning for multiview multilabel feature selection using fuzzy mutual information,” *IEEE Transactions on Cybernetics*, 2025.
- [30] J. Dai, W. Huang, C. Zhang, and J. Liu, “Multi-label feature selection by strongly relevant label gain and label mutual aid,” *Pattern Recognition*, vol. 145, p. 109945, 2024.
- [31] Y. Zhang and Y. Ma, “Sparse multi-label feature selection via dynamic graph manifold regularization,” *International Journal of Machine Learning and Cybernetics*, vol. 14, no. 3, pp. 1021–1036, 2023.
- [32] L. T. Vinh, S. Lee, Y.-T. Park, and B. J. d’Auriol, “A novel feature selection method based on normalized mutual information,” *Applied Intelligence*, vol. 37, no. 1, pp. 100–120, 2012.
- [33] X. Wu, Q.-G. Chen, Y. Hu, D. Wang, X. Chang, X. Wang, and M.-L. Zhang, “Multi-view multi-label learning with view-specific information extraction,” in *IJCAI*, 2019, pp. 3884–3890.
- [34] Z. Jiang, C. Li, Y. Jiang, Y. Ye, and X. Lu, “Global-affinity constraint with distillation-enhanced network for dual incomplete multi-view multi-label classification,” *Signal Processing*, p. 110190, 2025.
- [35] P. Hao, H. Zhang, and Y. Zhang, “Tensor-based opposing yet complementary learning for multi-view multi-label feature selection,” in *Proceedings of the 33rd ACM International Conference on Multimedia*, 2025, pp. 1822–1831.
- [36] P. Hao, K. Liu, and W. Gao, “Double-layer hybrid-label identification feature selection for multi-view multi-label learning,” in *Proceedings of the AAAI Conference on Artificial Intelligence*, vol. 38, no. 11, 2024, pp. 12 295–12 303.
- [37] P. Hao, K. Liu, and W. Gao, “Anchor-guided global view reconstruction for multi-view multi-label feature selection,” *Information Sciences*, vol. 679, p. 121124, 2024.
- [38] P. Zhu, Q. Hu, Q. Hu, C. Zhang, and Z. Feng, “Multi-view label embedding,” *Pattern recognition*, vol. 84, pp. 126–135, 2018.
- [39] X. Lu, S. Feng, G. Lyu, Y. Jin, and C. Lang, “Distance-preserving embedding adaptive bipartite graph multi-view learning with application to multi-label classification,” *ACM Transactions on Knowledge Discovery from Data*, vol. 17, no. 2, pp. 1–21, 2023.
- [40] Y. Zhang, J. Wu, Z. Cai, and P. S. Yu, “Multi-view multi-label learning with sparse feature selection for image annotation,” *IEEE Transactions on Multimedia*, vol. 22, no. 11, pp. 2844–2857, 2020.
- [41] R. Sanghavi and Y. Verma, “Multi-view multi-label canonical correlation analysis for cross-modal matching and retrieval,” in *Proceedings of the IEEE/CVF conference on computer vision and pattern recognition*, 2022, pp. 4701–4710.
- [42] P. Hu, L. Zhen, X. Peng, H. Zhu, J. Lin, X. Wang, and D. Peng, “Deep supervised multi-view learning with graph priors,” *IEEE Transactions on Image Processing*, vol. 33, pp. 123–133, 2023.
- [43] N. Timme, W. Alford, B. Flecker, and J. M. Beggs, “Synergy, redundancy, and multivariate information measures: an experimentalist’s perspective,” *Journal of computational neuroscience*, vol. 36, no. 2, pp. 119–140, 2014.
- [44] A. Beck and M. Teboulle, “A fast iterative shrinkage-thresholding algorithm for linear inverse problems,” *SIAM journal on imaging sciences*, vol. 2, no. 1, pp. 183–202, 2009.
- [45] J. Duchi, S. Shalev-Shwartz, Y. Singer, and T. Chandra, “Efficient projections onto the l_1 -ball for learning in high dimensions,” in *Proceedings of the 25th international conference on Machine learning*, 2008, pp. 272–279.

- [46] B. Jiang, C. Zhang, Y. Zhong, Y. Liu, Y. Zhang, X. Wu, and W. Sheng, "Adaptive collaborative fusion for multi-view semi-supervised classification," *Information Fusion*, vol. 96, pp. 37–50, 2023.
- [47] G. Tsoumakas, E. Spyromitros-Xioufis, J. Vilcek, and I. Vlahavas, "Mulan: A java library for multi-label learning," *The Journal of Machine Learning Research*, vol. 12, pp. 2411–2414, 2011.
- [48] A. Elisseeff and J. Weston, "A kernel method for multi-labelled classification," *Advances in neural information processing systems*, vol. 14, 2001.
- [49] M. Everingham, L. Van Gool, C. K. Williams, J. Winn, and A. Zisserman, "The pascal visual object classes (voc) challenge," *International journal of computer vision*, vol. 88, no. 2, pp. 303–338, 2010.
- [50] M. J. Huiskes and M. S. Lew, "The mir flickr retrieval evaluation," in *Proceedings of the 1st ACM international conference on Multimedia information retrieval*, 2008, pp. 39–43.
- [51] T.-S. Chua, J. Tang, R. Hong, H. Li, Z. Luo, and Y. Zheng, "Nus-wide: a real-world web image database from national university of singapore," in *Proceedings of the ACM international conference on image and video retrieval*, 2009, pp. 1–9.
- [52] P. Duygulu, K. Barnard, J. F. de Freitas, and D. A. Forsyth, "Object recognition as machine translation: Learning a lexicon for a fixed image vocabulary," in *European conference on computer vision*. Springer, 2002, pp. 97–112.
- [53] H. J. Escalante, C. A. Hernández, J. A. Gonzalez, A. López-López, M. Montes, E. F. Morales, L. E. Sucar, L. Villaseñor, and M. Grubinger, "The segmented and annotated iapr tc-12 benchmark," *Computer vision and image understanding*, vol. 114, no. 4, pp. 419–428, 2010.
- [54] M.-L. Zhang and Z.-H. Zhou, "Ml-knn: A lazy learning approach to multi-label learning," *Pattern recognition*, vol. 40, no. 7, pp. 2038–2048, 2007.
- [55] J. Demšar, "Statistical comparisons of classifiers over multiple data sets," *Journal of Machine learning research*, vol. 7, no. Jan, pp. 1–30, 2006.



Cheng Peng is currently working toward his Bachelor's degree in the College of Software, Jilin University, Changchun, China. His main research interests include feature selection, multi-label learning, multi-view learning, and information theory.



Yonghao Li received the Ph.D. degree from the College of Computer Science and Technology, Jilin University, in 2023. He joined the School of Computing and Artificial Intelligence, Southwestern University of Finance and Economics (SWUFE) in 2024. His research interests include feature selection, causal learning and federated learning. He has published more than 20 papers in renowned journals/conferences such as IEEE Transactions on Neural Networks and Learning Systems, IEEE Transactions on Artificial Intelligence, Pattern Recognition, Information Fusion, Knowledge and Information Systems, Information Processing & Management and IJCAI. He also serves as a reviewer for several journals and conferences, including TKDE, TNNLS, TKDD, TMM, TSMC, TCYB, TCSVT, TFS, TETCI, TCE, Pattern Recognition, Information Processing & Management, CVPR, ECCV, AAAI and ACM MM, etc.



Wanfu Gao (Member, IEEE) received the B.S. and Ph.D. degrees from the College of Computer Science and Technology, Jilin University, Changchun, China, in 2013 and 2019, respectively. He completed his postdoctoral research at the School of Artificial Intelligence, Jilin University, under the supervision of Prof. Yi Chang. He is an Associate Professor with the College of Computer Science and Technology, Jilin University. He has published more than 60 papers on feature selection, including SIGIR, ACL, AAAI, IJCAI, IEEE Transactions on Systems, Man, and Cybernetics: Systems, IEEE Transactions on Neural Networks and Learning Systems, IEEE Transactions on Artificial Intelligence, and Pattern Recognition. His research interests include feature selection, multilabel learning, and information theory. He serves on the program committees and as a reviewer for NeurIPS, ICML, AAAI, IJCAI, ICDM, TKDE, TNNLS, IEEE TCYB, and other conferences/journals. Dr. Gao received the 2019 ACM Changchun Doctoral Dissertation Award and the Postdoctoral Innovative Talents Support Program and was selected as a Top 2% worldwide scientist.



Jie Wen (Senior Member, IEEE) received the Ph.D. degree in Computer Science and Technology at Harbin Institute of Technology, Shenzhen in 2019. He is currently an Associate Professor at the School of Computer Science and Technology, Harbin Institute of Technology, Shenzhen. His research interests include image and video enhancement, pattern recognition, and machine learning. He has authored or co-authored more than 100 technical papers at prestigious international journals and conferences. He serves as an **Associate Editor** of *IEEE Transactions on Pattern Analysis and Machine Intelligence*, *IEEE Transactions on Image Processing*, *IEEE Transactions on Information Forensics and Security*, *IEEE Transactions on Circuits and Systems for Video Technology*, *Pattern Recognition*, and *International Journal of Image and Graphics*, an **Area Editor** of *Information Fusion*. He is on the **Editorial Board** of *Discover Artificial Intelligence and Mathematics*, and **Youth Editorial Board** of *CAAI Transactions on Intelligence Technology*. He also served as the **Area Chair** of *NeurIPS*, *ICLR*, *ACM MM*, and *ICML*, as well as the SPC of AAAI and *IJCAI*. He was selected for the 'World's Top 2% Scientists List' in 2021-2025. One paper received the 'distinguished paper award' from AAAI'23. For more information, please refer to the homepage: <https://sites.google.com/view/jerrywen-hit/home>.



Weiping Ding (Senior Member, IEEE) (M'16-SM'19) received the Ph.D. degree in Computer Science, Nanjing University of Aeronautics and Astronautics, Nanjing, China, in 2013. From 2014 to 2015, he was a Postdoctoral Researcher at the Brain Research Center, National Chiao Tung University, Hsinchu, Taiwan, China. In 2016, he was a Visiting Scholar at National University of Singapore, Singapore. From 2017 to 2018, he was a Visiting Professor at University of Technology Sydney, Australia. His main research directions involve deep neural networks, granular data mining, and multimodal machine learning. He ranked within the top 2% Ranking of Scientists in the World by Stanford University (2020-2025). He has published over 450 articles, including over 250 IEEE Transactions papers. His twenty authored/co-authored papers have been selected as ESI Highly Cited Papers. He serves as an Associate Editor/Area Editor/Editorial Board member of more than 10 international prestigious journals, such as IEEE Transactions on Neural Networks and Learning Systems, IEEE Transactions on Fuzzy Systems, IEEE/CAA Journal of Automatica Sinica, IEEE Transactions on Emerging Topics in Computational Intelligence, IEEE Transactions on Intelligent Transportation Systems, IEEE Transactions on Artificial Intelligence, Information Fusion, Information Sciences, Neurocomputing, Applied Soft Computing, Engineering Applications of Artificial Intelligence, Swarm and Evolutionary Computation, et al.